Flux noise probed with real time qubit tomography in a Josephson phase qubit

Daniel Sank[1], R. Barends[1], Radoslaw C. Bialczak[1], Yu Chen[1], J. Kelly[1], M. Lenander[1], E. Lucero[1], Matteo Mariantoni[1,5], A. Megrant[1], M. Neeley[1,4], P.J.J. O'Malley[1], A. Vainsencher[1], H. Wang[1,2], J. Wenner[1], T.C. White[1], T. Yamamoto[3], Yi Yin[1], A.N. Cleland[1,5], and John M. Martinis[1,5*]

[1] *Department of Physics, University of California, Santa Barbara, California 93106-9530, USA*
[2] *Department of Physics, Zhejiang University, Hangzhou 310027, China*
[3] *Green Innovation Research Laboratories, NEC Corporation, Tsukuba, Ibaraki 305-8501, Japan*
[4] *Lincoln Laboratory, Massachusetts Institute of Technology, Lexington, MA 02420-9108 and*
[5] *California NanoSystems Institute, University of California, Santa Barbara, CA 93106-9530, USA*

(Dated: June 8, 2012)

We measure the dependence of qubit phase coherence and flux noise on inductor loop geometry. While wider inductor traces change neither the flux noise power spectrum nor the qubit dephasing time, increased inductance leads to a simultaneous increase in both. Using our new tomographic protocol for measuring low frequency flux noise, we make a direct comparison between the flux noise spectrum and qubit phase decay, finding agreement within 10% of theory.

Superconducting qubits [1] are rapidly approaching the requirements needed for fault tolerant quantum computation, with recent experiments demonstrating a set of information storage, logic gates, and coherence improvements [2–5]. However, in recent demonstrations of both multi-qubit gates with phase qubits [6, 7] and error correction with transmons [8], the fidelity of the quantum process was limited by individual qubit dephasing times T_2. This dephasing results from low frequency fluctuations in the magnetic flux used to tune the devices' $|0\rangle \rightarrow |1\rangle$ transition frequency f_{10}. Traditionally, flux, transmon, and quantronium qubits have addressed this problem by idling at "sweet spots" where the first order sensitivity of device frequency to bias flux, $df_{10}/d\Phi$, is zero [9–11]. This approach has limitations, however, as qubits have to be moved from their idle points to participate in multi-qubit quantum gates. Furthermore, this approach to the flux noise problem constrains the qubit design space, as devices must be engineered to have a sweet spot.

Anomalous low frequency flux noise in superconducting devices has a long history in both experiment and theory [12–17]. Experiments with SQUIDs have found that the flux noise power spectral density $S_\Phi(f)$, which scales with frequency approximately as $1/f$, is insensitive to device size and materials; in fact no strong dependence on any device parameter has been found. Recent experiments have identified spins on the metal surfaces as the noise source [16, 17], but its exact microscopic mechanism remains unknown. Experiments with qubits have measured the dependence of dephasing on the bias point, characterized by $df_{10}/d\Phi$ [18–20], and have made direct low frequency [21] and indirect high frequency[22] measurements of the noise spectrum, but no experiment has carefully compared coherence with a direct measurement of the low frequency flux noise, nor has any experiment demonstrated a means of improving T_2 independently of the bias point.

In this Letter, we present a new tomographic protocol, which can be implemented in any two level system, for measuring low frequency fluctuations in the qubit precession frequency. With this protocol we present measurements of dephasing times and flux noise in phase qubits designed to improve T_2. In a circuit with increased inductance, we find an improvement in phase coherence at all bias points. We also use this protocol to make a clear and quantitative comparison between qubit dephasing and the measured noise spectrum. Finally, we report the first dependence of the flux noise on device geometry.

In order to motivate our qubit designs, we first review dephasing theory. Dephasing is caused by random fluctuations in the qubit's transition frequency f_{10}, characterized by a spectral density $S_{f_{10}}(f)$. For a Ramsey fringe experiment, the theoretical prediction for the time dependent decay of the qubit population probability is [23]

$$p(t) = \exp\left[-\frac{(2\pi)^2}{2}t^2\int_{f_\mathrm{m}}^{\infty} S_{f_{10}}(f)\left(\frac{\sin(\pi f t)}{(\pi f t)}\right)^2 df\right], \quad (1)$$

where f_m is a lower cutoff frequency equal to the inverse of the total experiment time [24, 27]. In phase qubits, frequency fluctuations are dominated by flux noise with a nearly $1/f$ spectral density, $S_\Phi(f) = S_\Phi^*/f^\alpha$, $\alpha \approx 1$ [21], resulting in a frequency noise spectral density $S_{f_{10}}(f) = (df_{10}/d\Phi)^2 S_\Phi^*/f^\alpha$. Inserting this into Eq. (1), performing the integral for the case $\alpha = 1$, and adding the contribution from energy loss (T_1), yields

$$\ln[p(t)] = -\frac{t}{2T_1} - \frac{(2\pi)^2}{2}t^2\left(\frac{df_{10}}{d\Phi}\right)^2 S_\Phi^* \ln\left(\frac{0.4}{f_\mathrm{m} t}\right). \quad (2)$$

The factor $\ln(0.4/f_\mathrm{m}t)$ is weakly dependent on t and has a numerical value of $\sim$24 in the experimental range $10\,\mathrm{ns} < t < 400\,\mathrm{ns}$ [27]. Defining the dephasing time T_2^*

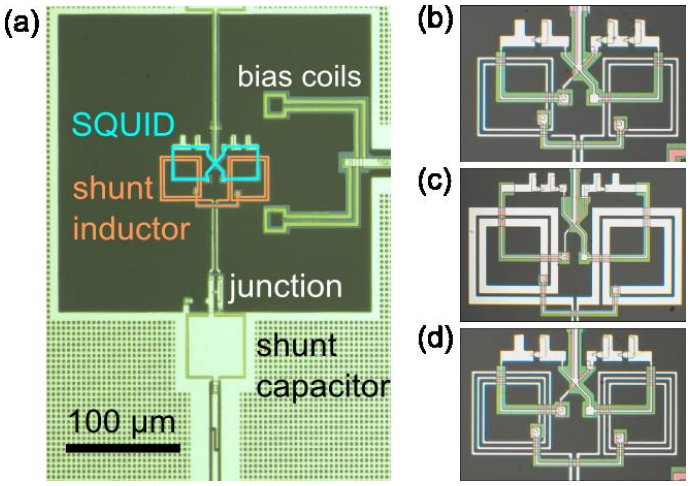

Figure 1: (color online) Phase qubit devices used in the experiments. Panel (a) shows the readout SQUID, inductor coils, bias coils, and shunt capacitor; panels (b), (c), and (d) show close-ups of the inductors and SQUIDs. Panel (b) shows the standard qubit coils, (c) the wide trace coils and (d) the high inductance coils. Horizontal image lengths are (b) 117μm, (c) 173μm, and (d) 123μm. Device parameters are given in Table I.

by the equation

$$\ln[p(t)] = -t/2T_1 - (t/T_2^*)^2, \tag{3}$$

we find

$$T_2^* \propto S_\Phi^{*-1/2} \left(\frac{df_{10}}{d\Phi}\right)^{-1} = S_\Phi^{*-1/2} L \left(\frac{df_{10}}{dI}\right)^{-1}, \tag{4}$$

where L is the inductance of the qubit loop and I is the loop current. Evidently T_2 can be increased by decreasing the sensitivity df_{10}/dI, but in the phase qubit this incurs a decrease in the qubit's nonlinearity Δ, defined as $\Delta \equiv f_{21} - f_{10}$. Nonlinearity is a critical figure of merit for qubits as greater nonlinearity allows for shorter control pulses and therefore more quantum gates during the qubit's lifetime [28]. We therefore re-express df_{10}/dI in terms of Δ according to $df_{10}/dI \propto \Delta^{3/4}$ [23], and substitute into Eq. (4), yielding

$$\ln(T_2^*) = -\frac{3}{4}\ln(\Delta) + \ln(L) - \frac{1}{2}\ln(S_\Phi^*) + K. \tag{5}$$

Here K depends on other device parameters, such as capacitance and junction critical current, which control the device's operating frequency range. As we do not wish to change the device frequency, K must remain fixed. Similarly, as we wish to improve T_2 without sacrificing nonlinearity, we regard Δ as a scaling parameter. There remain two ways to improve T_2^*: raise L or decrease S_Φ^*.

Each of these two methods was implemented though a redesign of the qubit inductor loop. The devices are pictured in Fig. 1 and parameters are given in Table I. The

Design	l [μm]	w [μm]	n	L [pH]
standard	296	1.5	2	710
wide	448	6.0	2	720
high L	456	1.5	3	1330

Table I: Device parameters for qubit inductors, each composed of two counter-wound coils. Each coil has total length l, trace width w, and n turns. The total inductance L includes both coils.

standard phase qubit [29, 30] is shown in Fig. 1a, with a close-up of the inductor coils in Fig. 1b. Coils of the first redesign are shown in Fig. 1c. Theories attributing flux noise to localized, uncorrelated magnetic moments of unpaired electron spins on the metal surfaces predict that S_Φ^* scales as R/W where R is the radius of the metal loop and W is its width [16, 21]. Therefore, to lower S_Φ^*, we increased the trace widths from the standard 1.5 μm to 6.0 μm. The second redesign is shown in Fig. 1d. In this device, we increase the inductance of the loop by adding turns, increasing from 710 pH to 1330 pH. Increased inductance should reduce noise currents driven by noise flux, increasing T_2^* as per Eq. (5).

In the first set of experiments we directly measure the flux noise. Previous experiments have used spin-echo type sequences to probe frequency fluctuations in the MHz range, but because these sequences are sensitive to time dependent fluctuations of the qubit frequency averaged over the entire data acquisition time they measure *integrals* of the noise spectral density. Consequently these works have assumed the noise to be $1/f$ and used the decay to estimate only the noise amplitude. In the work of Ref. [22] the noise was assumed to be $1/f^\alpha$ and the amplitude and exponent α were extracted at 0.1-10 MHz from Rabi and spin-echo type decays. To *directly* measure $S_\Phi(f)$ at *low* frequency, one can instead track the qubit frequency in real time and produce a spectrum with Fourier transform methods. A previous experiment with phase qubits implemented this idea by measuring the time dependent fluctuations of the position of the qubit resonance peaks [21]. The present experiment refines this idea: instead of measuring f_{10} spectroscopically, we use the free precession of the qubit state in the equator of the Bloch sphere. The angle traversed by the state in a fixed precession time τ is $\varphi = 2\pi f_{10}\tau$. By choosing τ and measuring φ tomographically we obtain f_{10}. Repetition of this measurement for several hours produces a time series $f_{10}(t)$. This measurement protocol, which we call the Ramsey tomography oscilloscope (RTO), is illustrated in Fig. 2. The RTO requires little calibration and is intrinsically stable as the tomographic measurement is insensitive to fluctuations in other parameters such as T_1 and measurement visibility.

The time series $f_{10}(t)$ is converted to a periodogram

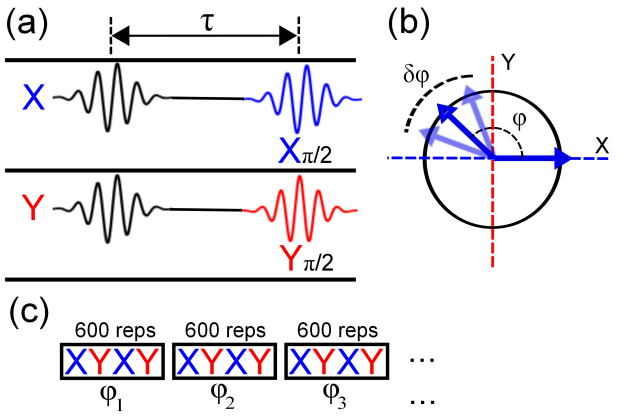

Figure 2: (color online) The Ramsey tomography oscilloscope (RTO) protocol. (a) Four Ramsey sequences are performed, two with the final $\pi/2$ pulse about the $\pm X$ axes, and two with the final $\pi/2$ pulse about the $\pm Y$ axes. The precession time for both sequences is fixed at $\tau =$ 100ns. (b) The combined X axis and Y axis sequences constitute tomography of the state in the x-y plane after precession by τ, thereby measuring the angle φ traversed by the state. (c) Several hundred subsequent X and Y measurements are grouped together to get an average value for φ. The entire process is repeated once per second for several hours to build up a time series $\delta f(t) = \delta\varphi(t)/2\pi\tau$.

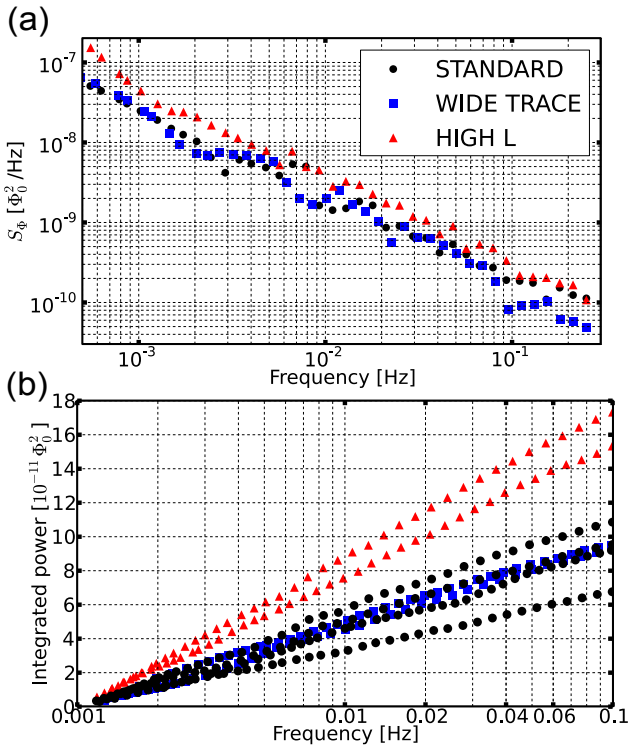

Figure 3: (color online) Power spectra for each inductor design. (a) Typical spectra for each type of device. (b) Spectral power integrated over the range 0.001 Hz to 0.1 Hz. In (a) we plot only one spectrum for each device design for clarity in the plot. In (b) we show several curves, measured at several bias points, in devices all fabricated on the same wafer.

using the discrete Fourier transform, and the result is appropriately normalized to produce the power spectral density of frequency noise $S_{f_{10}}(f)$ [27]. The sensitivity $df_{10}/d\Phi$ is measured separately, and the flux noise spectral density is obtained from the frequency noise spectral density according to $S_\Phi(f) = (df_{10}/d\Phi)^{-2} S_{f_{10}}(f)$. Results are shown in Fig. 3. Note in Fig. 3a that the spectra contain little statistical noise, in contrast to the data of Refs. [21, 22] where the measured power spectra wandered by almost an order of magnitude within each decade of frequency. Because the RTO yields a time series, we have direct access to the statistical distribution of the noise. We find that the distribution of low frequency noise closely follows a Gaussian curve [27].

The power spectra for each type of device scale as $f^{-1.1}$ over the measured band and have extrapolated amplitudes at 1 Hz between 3.5 and 5.0 $\mu\Phi_0/\sqrt{\text{Hz}}$. The spectra in Fig. 3a directly show that the high inductance device has more flux noise than the other two devices. Still, a clearer picture is obtained if we integrate the power spectral density to produce a plot of cumulative power [26]. From the integrated power shown in Fig. 3b, it is clear that the wide trace and normal designs have the same level of noise, while the high inductance device shows a 1.7× increase in noise power. The is our first main result: we find a dependence of the flux noise on the number of turns in the inductor loop.

We have also used the RTO to measure cross correlation in the noises of two phase qubits separated by 500 μm on the same chip. We find that the measured correlation is no greater than that found for two independently simulated $1/f$ noise signals [27].

For the wide trace design, the lack of change in noise level predicts that T_2^* will remain the same as the standard design. For the high inductance design, the 1.3× increase in noise amplitude and the designed inductance increase of 1.87×, predict via Eq. 5 an increase in T_2^* of 1.4×.

In the second set of experiments we measured T_2^* at several flux bias points that varied Δ. The exponential energy decay time T_1 and nonlinearity Δ are first measured in separate experiments [31, 32]. We then measure a Ramsey decay curve and fit the data to Eq. (3) so that the contribution from T_1 is appropriately removed in obtaining the Gaussian decay constant T_2^*.

The results shown in Fig. 4 reveal that the dependence of the extracted values of T_2^* on Δ is consistent with the expected -3/4 power law. This indicates that T_2^* scales inversely with $df_{10}/d\Phi$ as predicted by Eq. (4), supporting our assumption that the noise is dominated by flux. The wide trace devices show no difference in T_2^* from the standard design, consistent with the fact that the inductances and measured flux noise are the same in those two designs. The high inductance device showed an increase

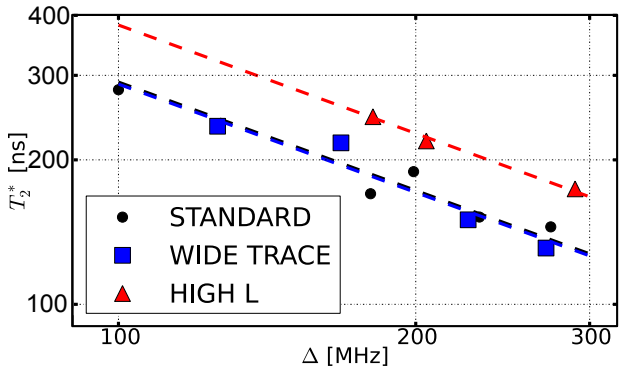

Figure 4: (color online) Plot of Ramsey decay time T_2^* vs. nonlinearity Δ for each type of device. Each point comes from a fit to Eq. (3). For each bias flux, T_1 and Δ are measured in separate experiments. Dashed fit lines are drawn with the predicted slope of $-3/4$ in order to compare magnitudes. The fit lines for the standard and wide trace designs fall on top of one another. The high inductance devices show an increase in T_2^* by a factor of 1.3. Confidence bounds, typically 2% of data values, cannot be seen on this scale.

in T_2^* by 1.3× relative to the standard design, reasonably close to the 1.4× increase predicted above. This is our second main result: increased inductance improves the qubit's dephasing time independently of the bias point, and without sacrificing any other figure of merit.

The scaling of the noise power with inductance, and the lack of scaling with trace aspect ratio, have implications for models of the flux noise. The wide trace design has 1.5× greater coil length and 4× greater trace width than the standard design, but no change in noise in agreement with previous experiments on SQUIDs [12]. This is incompatible with models predicting $S_\Phi^* \propto R/W$, such as the independent surface spins proposed in Ref. [21], or single electrons interacting via the superconducting condensate as proposed in Ref. [14]. This could indicate a correlation length larger than the trace width. On the other hand, the high inductance design, with the same fractional coil length increase as the wide trace devices, had a 1.7× increase in noise power. The similarity of measured noise in flux and phase qubits, with coil lengths differing by several orders of magnitude, make it unlikely that this change is due to the coil length. On the other hand, our increased length was implemented by adding an extra turn to the coil, which has not been tested before. A simple model assuming that the noise from each coil turn adds incoherently would predict that the high inductance design should produce 1.5× more noise than the standard. If we additionally account for small inter-turn coupling due to the slightly non-local fields of dipole sources, along with the non-uniform distribution of current in the superconducting traces [21], this number increases to 1.6×, in close agreement with our data.

Thus far we have discussed the *relative* dephasing times and flux noise levels. It remains to check whether the the *absolute* measured noise levels accounts for the observed dephasing times. This is done by comparing the value of $S_\Phi^{*\mathrm{Ramsey}}$ extracted from a fit to the Ramsey data with the value $S_\Phi^{*\mathrm{RTO}}$ found directly using the RTO [25]. Note that previous experiments with qubits have been unable to make this comparison because an accurate measurement of the flux noise was unavailable. As described by Eq. (1) and the surrounding discussion, the exact form of the Ramsey fit function depends on the scaling power α. In particular, it would be inappropriate to fit the Ramsey data to Eq. (2); that equation was derived under the assumption that α is equal to 1, whereas we found in the RTO that α is closer to 1.1. To take the scaling power into account properly, we numerically evaluate the integral in Eq. (1) for $\alpha = 1.1$, and use the resulting fit function to extract $S_\Phi^{*\mathrm{Ramsey}}$ [27]. For all devices and bias points we find that the values of $S_\Phi^{*\mathrm{Ramsey}}$ extracted in this way agree with $S_\Phi^{*\mathrm{RTO}}$ to within 10%. We emphasize that properly accounting for the *measured* slope of the noise spectral density when fitting the Ramsey curves is essential in obtaining agreement between the Ramsey and RTO experiments. For example, if we take $\alpha = 1$ we find $S_\Phi^{*\mathrm{Ramsey}} \approx 4\, S_\Phi^{*\mathrm{RTO}}$.

In conclusion, we have found that increased loop inductance is a viable means to improve superconducting qubit phase coherence independently of bias point. We have introduced the RTO protocol for directly measuring flux noise, and used this protocol to make a direct comparison between measured flux noise and qubit dephasing times. There we find that the noise level extracted from Ramsey decay agrees with the direct measurement only when the exact slope of the noise spectrum is considered. Using the RTO we compared the flux noise in devices with widened traces and increased number of inductor turns. With no change found in the wide traces, but an increase in noise with number of turns, we suggest that the noise sources may be correlated over distances greater than the 6 μm trace width, but smaller than the 400 μm length of the inductor coils. Clearly, the correlation length of the flux noise sources is a key parameter that should be studied in further experiments.

We thank Robert McDermott for discussions on flux noise in superconductors. This work was supported by Intelligence Advanced Research Projects Activity (IARPA) under ARO award W911NF-08-1-0336 and under Army Research Office (ARO) award W911NF-09-1-0375. M. M. acknowledges support from an Elings Postdoctoral Fellowship. RB acknowledges support from the Rubicon program of the Netherlands Organization for Scientific Research. Devices were made at the University of California Santa Barbara Nanofabrication Facility, a part of the NSF-funded National Nanotechnology Infrastructure Network.

* Electronic address: martinis@physics.ucsb.edu

[1] J. Clarke and F. K. Wilhelm, Nature **453** (2008).

[2] L. DiCarlo, M. Reed, L. Sun, B. Johnson, J. Chow, J. Gambetta, L. Frunzio, S. Girvin, M. Devoret, and R. Schoelkopf, Nature **467**, 574 (2010).

[3] M. Neeley et al., Nature **467**, 570 (2010).

[4] H. Wang et al., Phys. Rev. Lett. **106**, 060401 (2011).

[5] H. Paik et al., arXiv:1105.4652 (2011).

[6] R. C. Bialczak et al., Nature Phys **6**, 409 (2010).

[7] M. Mariantoni et al., Science **334**, 61 (2011).

[8] M. Reed, L. DiCarlo, S. Nigg, L. Sun, L. Frunzio, S. Girvin, and R. Schoelkopf, arXiv:1109.4948 (2011).

[9] I. Chiorescue, Y. Nakamura, C. J. P. M. Harmans, and J. E. Mooij, Science **299** (2003).

[10] J. Koch, T. M. Yu, J. Gambetta, A. A. Houck, D. I. Schuster, J. Majer, A. Blais, M. H. Devoret, S. M. Girvin, and R. J. Schoelkopf, Phys. Rev. A **76**, 042319 (2007).

[11] D. Vion, A. Aassime, A. Cottet, P. Joyez, H. Pothier, C. Urbina, D. Esteve, and M. H. Devoret, Science **295** (2002).

[12] F. C. Wellstood, C. Urbina, and J. Clarke, Appl. Phys. Lett. **50** (1987).

[13] S.K. Choi, D.-H. Lee, S. G. Louie, and J. Clarke, Phys. Rev. Lett. **103**, 197001 (2009).

[14] L. Faoro and L. B. Ioffe, Phys. Rev. Lett. **100**, 227005 (2008).

[15] R. H. Koch, D. P. DiVincenzo, and J. Clarke, Phys. Rev. Lett. **98**, 267003 (2007).

[16] S. Sendelbach, D. Hover, A. Kittel, M. Mück, J. M. Martinis, and R. McDermott, Phys. Rev. Lett. **100**, 227006 (2008).

[17] S. Sendelbach, D. Hover, M. Mück, and R. McDermott, Phys. Rev. Lett. **103**, 117001 (2009).

[18] F. Yoshihara, K. Harrabi, A. Niskanen, Y. Nakamura, and J. S. Tsai, Phys. Rev. Lett. **97** (2006).

[19] G. Ithier et al., Phys. Rev. B **72**, 134519 (2005).

[20] K. Kakuyanagi, T. Meno, S. Saito, H. Nakano, K. Semba, H. Takayanagi, F. Deppe, and A. Shnirman, Phys. Rev. Lett. **98**, 047004 (2007).

[21] R. C. Bialczak et al., Phys. Rev. Lett. **99**, 187006 (2007).

[22] J. Bylander, S. Gustavsson, F. Yan, F. Yoshihara, K. Harrabi, G. Fitch, D. G. Cory, Y. Nakamura, J.-S. Tsai, and W. D. Oliver, Nature Phys **7**, 565 (2011).

[23] J. M. Martinis, S. Nam, J. Aumentado, K. M. Lang, and C. Urbina, Phys. Rev. B **67**, 094510 (2003).

[24] This formula was derived in [23] as an approximation for the case of small noise. It is exact for Gaussian noise.

[25] The comparison should technically be made between values of frequency noise rather than flux noise as the scale factor $d_{10}/d\Phi$ drops out. Since frequency noise in phase qubits has been found to be flux dominated in Ref. [21] the discussion in terms of flux noise is justified.

[26] To avoid complications from aliasing and spectral leakage from DC, we omit the upper and lower edges of the measured frequency band, integrating only over the range 10^{-3} to 10^{-1} Hz where the measurement is the least susceptible to these effects [33].

[27] See supplemental material.

[28] E. Lucero, M. Hofheinz, M. Ansmann, R. C. Bialczak, N. Katz, M. Neeley, A. D. O'Connell, H. Wang, A. N. Cleland, and J. M. Martinis, Phys. Rev. Lett. **100**, 247001 (2008).

[29] J. M. Martinis, Quantum Information Processing **8**, 81 (2009).

[30] M. Neeley, M. Ansmann, R. C. Bialczak, M. Hofheinz, N. Katz, E. Lucero, A. O'Connell, H. Wang, A. N. Cleland, and J. M. Martinis, Phys. Rev. B **77**, 180508 (2008).

[31] J. M. Martinis, S. Nam, J. Aumentado, and C. Urbina, Phys. Rev. Lett. **89**, 117901 (2002).

[32] E. Lucero et al., Phys. Rev. A **82**, 042339 (2010).

[33] F. J. Harris, Proc. IEEE **66**, 51 (1978).